Plant, Cell & Environment

WILEY

Plant, Cell & Environment

ORIGINAL ARTICLE OPEN ACCESS

Light Limitation and Foliar Pathogenic Infection Impact Phloem Anatomy and Function in *Pinus radiata* D. Don

Mireia Gómez-Gallego[1,2] | Damien Sellier[2] | Alan Dickson[2] | Martin K.-F. Bader[3] | Sebastian Leuzinger[4] | Nari Williams[5,6]

[1]Université de Lorraine, INRAE, UMR IAM – Interactions Arbres-Microorganismes, Nancy, France | [2]New Zealand Forest Research Institute (Scion), Rotorua, New Zealand | [3]Maastricht University, System Earth Science, Venlo, The Netherlands | [4]School of Science, Auckland University of Technology, Auckland, New Zealand | [5]The New Zealand Institute for Plant & Food Research Limited, Havelock North, New Zealand | [6]The University of Auckland, School of Biological Science, Auckland, New Zealand

Correspondence: Mireia Gómez-Gallego (mireia.gomez-gallego@inrae.fr)

Received: 19 February 2025 | **Revised:** 28 April 2025 | **Accepted:** 29 April 2025

Funding: This study was supported by the MBIE research programme 'Healthy Trees Healthy Future' (C04X1305) and by the joint PHC/Dumont d'Urville (DDU-FRI1601) fund.

Keywords: conifer | environmental plasticity | foliar disease | light availability | Monterrey pine | nonstructural carbohydrates | permeability | phloem transport | sieve cells | sink limitation

ABSTRACT

Phloem plays a major role in plant physiology, health and growth. However, little research has addressed the impact of biotic and abiotic stressors on phloem structure and development. This study extends recent interest on stress impact on phloem to further understand its physiological limits by exploring a common combination of stressors within forest systems: reduced light availability and concomitant foliar pathogenic infection. We compared juvenile *Pinus radiata* D. Don. plants growing under optimal light conditions to plants growing under reduced light availability and exposure to pathogenic infection. We monitored foliar gas exchange and took destructive samples for nonstructural carbohydrate (NSC) analysis and phloem anatomy in spring and early summer. We used software-assisted image analysis to determine cell composition and area of conducting phloem, and a fluid dynamics model to derive phloem hydraulic parameters. Phloem showed environmental plasticity within the same growing season. We found changes in phloem anatomy in shaded and infected plants, including an increased sieve cell density and permeability, and reduced cell wall thickness. While intrinsic phloem hydraulic efficiency was maintained at the tissue level in stressed plants, the reduction in phloem cross-sectional area resulted in an eventual decline in phloem sap flow rate. Thus, phloem cross-sectional area was dynamically adjusted to match reduced translocation requirements. In addition, shaded and infected plants experienced reduced growth and C assimilation, as well as greater necrotic photosynthetic tissue, but showed similar levels of total NSC than control plants. The high levels of NSC observed in our stressed plants are an important finding that suggests that radial growth cessation and, by association, phloem formation impairment are induced by sink limitation instead of reduced carbohydrate supply to the meristem.

1 | Introduction

Phloem is essential to tree function, serving as the primary transport system for photoassimilates, which are translocated and distributed to sink tissues throughout the tree. Its sieve elements, the specialised conductive cells, also transport minerals, organic acids and amino acids (Ziegler 1975). Sap movement in the phloem has been hypothesised almost a century ago to operate as a pressure flow (Münch 1930). The osmotic pressure differential drives the flow of sugars from source to sink tissues, where they are retrieved from the vascular system and consumed, thus maintaining an osmotic potential gradient. That hypothesis, which has received strong experimental support (Knoblauch et al. 2016), implies that assimilate transport is a predominantly passive mechanism, requiring no energy expenditure and with allocation passively prioritised by sink activity (Minchin et al. 1993). Another equally-important consequence of the pressure-flow hypothesis is that, while there is biological control to regulate osmotic potential along the phloem (Thompson and Holbrook 2003), translocation rates are predetermined by phloem hydraulic conductivity, which depends only on its size and anatomy. It follows that phloem structure and dimensions must scale within the plant (Hölttä et al. 2013; Jyske and Hölttä 2015) and across species (Jensen et al. 2011) to ensure transport efficiency, that is, transport rates matching sink demand over long distances and in different environments. The dependency of transport on conduit's properties has enabled methods relying on anatomical sampling and hydraulic theory to evaluate sap velocity (Jensen et al. 2012; Mullendore et al. 2010) or carbon translocation rates of forest trees (Epron et al. 2019b) without requiring the direct measurement of phloem sap flow, a reputedly complex and error-prone process.

In addition to transport of photoassimilates, phloem plays a critical role in induced defence mechanisms through the translocation of defensive metabolites and signals including hormones, RNA and proteins from stress-affected tissues (Heil and Ton 2008; Van Bel et al. 2013). Several plant pathogens utilise vascular tissues to reach distant organs within the plant; with some, the phloem-limited pathogens, being specialised to the unique phloem environment (Bendix and Lewis 2018; Malinowski et al. 2024). Therefore, phloem is the concourse of multiple processes that are crucial for tree responses to both abiotic and biotic stress. Despite its key role, the impact of stressing environmental conditions on phloem physiology has been understudied. The main challenge lies in the inherent complexity and inaccessibility of this tissue: sieve elements operate under pressure, and are easily altered during sampling and difficult to isolate. However, new methods have been developed, that enhance the study of phloem (Epron et al. 2019a; Sevanto 2019).

The limited studies on the effects of environmental constraints on phloem function have predominantly focused on the impact of drought. From those, we have learnt that trees strive to maintain the homoeostasis of phloem transport for as long as they can, highlighting the ultimate importance of this tissue for tree function (Salmon et al. 2019). Environmental constraints other than drought may influence phloem physiology as well and their study will provide further insights into the phloem's ecological role and the physiological limits of phloem transport (Epron et al. 2019a). Two examples of concurrent stressors are light limitation and biotic agents. Insect and pathogenic attacks offer a wide range of study cases as they can impact phloem tissue either directly, namely sap-suckers and phloem-limited pathogens; or indirectly, such as root rot and foliar pathogens and herbivores. The impacts of biotic stressors and reduced light availability on tree physiology are generally well-known. Foliar pathogens have been reported to reduce CO_2 assimilation (Bassanezi et al. 2002; Bauer et al. 2000; Berger et al. 2007; Ganthaler et al. 2014; Hajji et al. 2009; Manter et al. 2000; Pinkard and Mohammed 2006), and both radial and linear growth (Bert et al. 2016; Ganthaler et al. 2014; Gibson 1972; Manter et al. 2003), and to lead to active storage of NSC particularly in the crown (Martínez-Vilalta 2014; Saffell et al. 2014). Light availability has a direct impact on a tree's gas exchange system, leaf traits and growth. A reduction in light-saturated photosynthetic capacity (A_{max}) and in nitrogen content per leaf area, and an increase in specific leaf area (*SLA*) have been reported for decreasing values of light (Bond et al. 1999; Niinemets 2007; Zhang et al. 2016). In addition, growth suppression has been observed in shade-grown trees compared to open-grown trees (Yasuda et al. 2018).

Light limitation and foliar pathogenic infection constitute a common stress combination in forest ecosystems which often co-occur, especially for dominated trees and regenerating saplings (Brown and Heckman 2021). Typically, foliar pathogen infection is greater on leaves in the lower parts of the tree canopy that experience lower light levels (Brown and Heckman 2021). This can be explained by: higher leaf wetness of shaded leaves (Pinon et al. 2006); higher *SLA* values of shaded leaves that are associated with lower resistance to pathogens (Poorter et al. 2009; Toome et al. 2010); and reduced constitutive and induced secondary metabolites under light limitation (Huang et al. 2020). Thus, in shaded subcanopy conditions, the main agents of seedling mortality are pathogen and herbivore attacks. Carbon allocation patterns are optimised to fulfil defence and storage needs to facilitate recovery from tissue loss, at the expense of growth (Imaji and Seiwa 2010; Kurokawa et al. 2004). Therefore, one of the impacts of light limitation and foliar pathogenic attack is growth reduction.

While we have prior knowledge of how shade and foliar pathogenic infection affect gas exchange, growth and carbon allocation, their impact on phloem function and anatomy remains unexplored. To the best of our knowledge, there is only one study that addresses the impact of light exposure on the ratios of xylem-to-leaf area and phloem-to-leaf area in branches (Zhang et al. 2016). The authors showed that, in a range of broad-leaf tree species, those ratios were not affected by light conditions but by the shade tolerance of the species. However, they found that leaf, xylem and phloem areas were larger in sunlit branches than in shaded ones. In the present study, we aimed to explore the impacts of shade and foliar pathogenic infection on phloem structure and function in a previously undescribed conifer species. We chose *Pinus radiata* D. Don which is a fast-growing species and used worldwide in forest plantations. Radiata pine has an intermediate tolerance to shade (Warrington et al. 1989) and can be infected by a range of foliar pathogens, namely *Phytophthora pluvialis*, *P. kernoviae*, *Dothistroma septosporum*, *D. pini* and *Cyclaneusma minor*, with partly similar symptoms (Bulman 1993; Fraser et al. 2020; Gómez-Gallego et al. 2017). We sought to quantify to what extent the phloem can respond to those stressors (lack of light and foliar pathogenic infection) and scale dynamically to translocation requirements through adaption in size, cellular structure and hydraulic efficiency. To address the question, we studied *P. radiata* plants of a susceptible genotype grown under full light conditions and in the understory of a radiata pine plantation forest with the presence of *Dothistroma* spp. and *Phytophthora pluvialis* and *P. kernoviae*, to get naturally infected light-limited plants. We developed a pipeline consisting of a semi-automated image analysis procedure to identify individual cell geometry and type in the conductive phloem and a fluid dynamics model to provide theoretical estimates of translocation rates for a given anatomical structure. We monitored gas exchange and destructively sampled NSC in needles, stems, roots, and the phloem tissue, in spring and early summer, to assess phloem plasticity under light limitation and foliar pathogenic infection in the same growing season in the context of whole-plant functioning. As the shade treatment consisted of a strong reduction of the available light, we hypothesised that shaded plants would present minimally functional phloem which would be narrowed and present a reduced number of sieve cells and axial parenchyma cells than the phloem of sunlight plants. We also expected a reduced amount of assimilated carbon, and an accumulation of NSC on the needles to respond to the defence sink created by the foliar pathogenic infection.

2 | Material and Methods

2.1 | Plant Material and Treatment Description

Pinus radiata scions from a genotype susceptible to the red needle cast disease were taken from mature trees, grafted on 1-year-old rootstock, and grown in 10 L buckets during 1 year before the experiment started. The grafts were kept in the same buckets for the duration of the experiment. We placed 16 grafts under full sunlight conditions (control plants) in the Scion nursery (Rotorua, New Zealand), and another 19 grafts in the understory of a mature *P. radiata* plantation (−38.345842, 176.004822, Kinleith forest, New Zealand) under reduced light availability (light-limited plants) and in a red-needle-cast infected area on September 1, 2017. The plants were not transplanted, but placed at these two locations in their pots. After 1 month (October 2), we sampled nine plants from each treatment. This sampling time is referred to as 'spring' hereafter. After 5 weeks (November 7), the rest of the field-grown grafts in their pots had to be moved to another forest site that was less than 8 km apart from the first site (−38.363292, 175.918193, Kinleith forest, New Zealand). This site had the same light-limiting conditions (Figure 1) and similar pathogenic infection occurrence. After 6 weeks (December 20), the remaining control (7 plants) and light-limited infected plants (10 plants) were sampled. This sampling time is referred to as 'summer' hereafter. Height and diameter of each sapling were measured at the start of the experiment (September 1) and again at the time they were sampled, either spring or summer, to determine the growth increments for the corresponding period.

The two study locations in central North Island of New Zealand present a temperate oceanic climate (Cfb, according to Köppen's climate classification) with temperature of coldest month averaging above 0°C, all-month average temperature below 22°C, and with no significant precipitation difference between seasons (Köppen 1936). This climate enables an expanded growing season of radiata pine in New Zealand, with partial winter dormancy. While the cambium is active from mid-July until late May the following year, with minimum activity in the

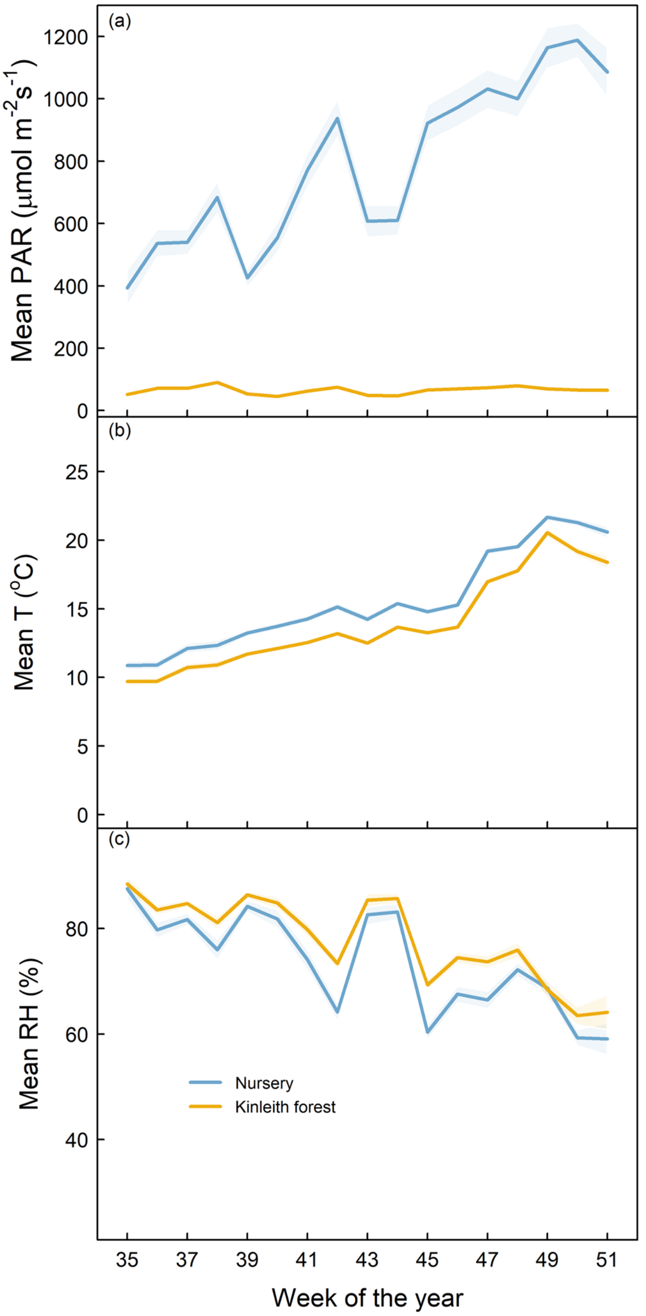

FIGURE 1 | Characterisation of the study sites: (a) mean *PPFD* (μmol m^{-2} s^{-1}) from 8 a.m. to 6 p.m.; (b) mean temperature (°C) and (c) mean relative humidity (RH) for each site during the whole study period (from September 1 to December 20, 2017).

southern hemisphere winter solstice (June 21, day of the year 172), cambial cell division peaks in spring and early summer (Nanayakkara et al. 2019; Tennent 1986). We sampled thus during the period with higher cambial activity. While climate trends are the same, we note that there were slight differences in air relative humidity and temperature between the two growing conditions, linked to the treatments themselves (Figure 1). Subcanopy conditions inherently implied slightly higher relative humidity and slightly cooler temperatures than full sunlight conditions, integrating the characteristics of natural forest environments.

2.2 | Gas Exchange and Chlorophyll Fluorescence Measurements

All gas-exchange and chlorophyll fluorescence measurements were taken on attached, asymptomatic, 1-year-old needles on lateral shoots. We took two measurements per plant, from the upper (first whorl) and bottom (second whorl) half of the crown. Previous to measurements, rapid light response curves of the apparent electron transport rate (*ETR*) were measured in five plants using an Imaging-PAM chlorophyll fluorometer (M-series, Walz, Effeltrich, Germany; Rascher et al. 2000) to derive the saturating level of the photosynthetic photon flux density ($PPFD_{sat}$). At each sampling date, we measured the following parameters, from two fascicles from each of the two labelled shoots, under light-saturating conditions ($PPFD_{sat}$ of 770 μmol m^{-2} s^{-1}): light-saturated net photosynthetic rate (A_{max}), stomatal conductance (g_s), effective quantum yield (Φ) and *ETR*. For those measurements, we used a coupled chlorophyll fluorescence and gas-exchange system (Imaging-PAM M-Series and GFS-3000, Walz, Effeltrich, Germany). The cuvette conditions were kept at 400 ppm CO_2 concentration, 20°C temperature and 60% relative humidity. All the measurements were performed between 8 a.m. and 12.30 pm.

2.3 | Nonstructural Carbohydrates

After each gas-exchange measurement, for NSC determination, we collected the two fascicles from the upper crown used for the gas exchange measurements. We also cut two 2-mm thick stem discs 2 cm above the graft union. We removed the bark to analyse only NSC content in sapwood. Fine and coarse roots (ca. 50% each) were cut, washed and rinsed. All samples were frozen at −80°C at the time of sampling using liquid nitrogen, before overnight lyophilization using a FreeZone Freeze Dry System (Model 7934037, Labconco, Kansas City, Missouri, US). Needle samples were added to 4-mL grinding metal balls (SPEX) and then ground to fine powder using a GenoGrinder 2010 (SPEX SamplePrep, Stanmore, UK). Stem and root samples were ground in impact-resistant 2-mL tubes containing 2-mm glass beads and 2-mm yellow zirconium oxide beads (Lysing Matrix H, MP Biomedicals, Auckland, New Zealand) using a bead mill homogeniser (Omni bead ruptor 24, Omni International, Kennesay, Georgia, US). We quantified NSC concentration following the procedure published at (Gomez-Gallego et al. 2020) using the reflectance spectra from 1300 to 2650 nm to estimate NSC concentrations (Ramirez et al. 2015).

2.4 | Sample Collection, Preparation and Image Analysis

2.4.1 | Sample Collection and Preparation

Three-cm long stem sections were cut at 2.5 cm above the graft union. The samples were immediately immersed in FAA fixative (50% ethanol, 5% (v/v) acetic acid, 3.7% (v/v) formaldehyde) in 50-mL tubes. The samples were placed in ethanol before being transferred to LR White (Hard grade) resin (Proscitech, Australia) and infiltrated overnight under vacuum to remove air bubbles. They were then placed in 30 mm diameter disposable moulds ('KM' acrylic moulds—Presi, Grenoble, France). The moulds were polymerised at 60°C overnight. The polymerised resin block was not removed from the mould, and the entire block was mounted in the sample holder and ground down and polished using a Presi Mecapol P230 grinding unit. A range of grinding papers were used ranging from a 320 grit (coarse, for grinding to the appropriate image plane) to a 4000 grit (smooth, for polishing to a mirror finish). A few drops of 0.01% (aqueous) calcofluor white (American Cyanamid Company, Bound Brook, N.J., USA) were placed on the block surface for 2 min before being rinsed off in water. Imaging was performed using an upright Leica TCS SP5 II confocal laser scanning microscope (Leica Microsystems, Germany). Excitation was at 355 (UV) and 488 nm (blue), and emission bandwidths were 400–480 (blue), 492–537 (green), and 625–800 nm (red). A 20× glycerol immersion lens was used at 2× zoom giving an approximate image area of 380 × 380 μm^2.

2.4.2 | Image Processing and Cell Identification

Image processing was performed using ImageJ 1.52 h (Abramoff et al. 2004). The blue (400–480 nm) channel was used to determine the cell dimensions. The ImageJ resident Euclidean Distance Map (EDM) method was used to generate Voronoi cells around the binarised cell lumens to find the mid-point between adjacent wood cells. It was assumed that this mid-point was synonymous with the middle lamella and that the boundary defined by the Voronoi cell also defined the perimeter. The mean cell-wall thickness was determined from the mean distance weighted intensity value defining the cell perimeter (Dickson et al. 2017). The full colour image (red, green and blue channels) was used to assign a type to each cell present in the conductive phloem using visual criteria. The phloem refers to the functioning part of the tissue only hereafter.

We could not distinguish between cells formed during previous and current growing season, because of the apparent lack of tangential parenchyma banding in the species, a marker traditionally used in other species to study tissue ring structure (Gričar et al. 2021). Additionally, final markers of growth increment boundaries based on the transition from narrow late-phloem to wide early-phloem SC were absent (Angyalossy et al. 2016). One of the underlying causes for this indeterminate pattern in SC size could be the year-long growing season for *P. radiata* (Tennent 1986) with no winter dormancy in New Zealand (Barnett 1971) and a consequent smooth transition in cell size and cell wall thickness as cambial activity continues from autumn to spring. However, our sampling period covered the maximum cambial activity in New Zealand (Nanayakkara et al. 2019). We assumed the bias of possibly including a few previous-year cells, as they must have been relatively low in number and proportion respect to newly formed cells. In addition, plants were grown under the same exact conditions before the onset of treatments. Thus, differences could primarily be attributed to the treatments.

We defined four cell types (Table 1): axial parenchyma (AP), tannin-filled parenchyma (TP) ray parenchyma (R) cells and sieve cells (SC).

TABLE 1 | Visual characteristics of phloem individual cells used for classification.

Cell type	Decision criteria
Sieve cell	Low to medium cytoplasmic content (green); cytoplasmic content tends to be parietal; presence of central cavity; absence of nucleus.
Ray parenchyma	Radially elongated; high cytoplasmic content; presence of nucleus; thin wall; part of a radial file.
Axial parenchyma	Medium to high cytoplasmic content; cytoplasmic content diffuse; thin wall. Strasburger cells would be identified as this cell type.
Tannin cell	Has orange content.
Undetermined	Presents features that belongs to several other types; has indeterminate features; specular highlights in lumen?
Not a cell	Inter cellular space; artefact of shape detection algorithm; within the functional phloem region
Outside	Any cell or shape outside the functional phloem region: sieve cell with concave or buckled wall, distorted ray element; tannin cell surrounded by distorted cells or cells with high aspect ratio; differentiating sieve cell adjacent to cambium and smaller than cells on the left.

2.5 | Data Analysis

All statistical computations and graphics were performed using R software version 4.2.3 (R Core Team 2023).

The $PPFD_{sat}$ was determined to be 0.9 per the value of the asymptote. We fitted the asymptotic function on the data of the rapid light curves where *PPFD* was lower than 1000 µmol·m^{-2}·s^{-1}, as *ETR* started to decrease at higher values of *PPFD*. We also fitted a generalised additive mixed model (*gamm* function, *mgcv* package in R), with *ETR* as a response variable, *PPFD* as a predictor, and plant identity as a random factor to predict *ETR* from *PPFD*. We evaluated the impact of subcanopy growing conditions on light by analysing the measured light in the two weather stations. We computed the kernel density estimates of *PPFD* measured hourly selecting the range from 6 am to 8 pm during the experiment with the function *density* in R. We calculated the integrated difference in density of *PPFD* values in the range from 205 to 1408 µmol·m^{-2}·s^{-1} (which corresponded to an *ETR* higher than 30 µmol electrons·m^{-2}·s^{-1} according to the measured rapid light curves), between the nursery and the field site. This allowed to quantify the differences in light availability and its impact on gas exchange.

To see which variables were most affected by the treatments, we pooled the data on phloem anatomy and hydraulics, NSC content and gas exchange. A total of 86 variables were considered (Table S1). As the number of variables is higher than the observations ($n = 35$), we used the Elastic Net algorithm to obtain a selection of parameters that better predicted whether a plant has experienced the environmental constraints or belongs to the control growing conditions. First, we performed a leave-one-out cross-validation for our data set to optimise the penalty parameters, lambda and gamma (function *cv. glmnet*, package *glmnet*). Then, we run the optimal algorithm to obtain the selected variables (function *glmnet*). We used the standardised values of the 86 variables as an input to the Elastic Net analysis. The Elastic Net algorithm does not output p values, but the parameter estimates. Therefore, we ran a generalised linear model (*glm* R function, using the binomial family) with each selected variable as a predictor of the treatment (control or subcanopy-grown). We calculated the explained deviance of each individual model as $1 - \frac{deviance}{null\ deviance}$, and corrected the p value of each variable (*p.adjust* R function) using the BH method (Benjamini and Hochberg 1995). Finally, we modelled each selected variable as a function of the treatment (control or subcanopy-grown) and the sampling date (spring or summer) using linear models, or generalised linear models if the response variable did not follow a normal distribution (*lm* function or *glm* function, respectively), to evaluate the impact of environmental constraints and the season on anatomical and hydraulic phloem parameters, gas exchange variables and nonstructural carbohydrates.

2.6 | Hydraulic Properties

2.6.1 | Permeability

We assumed that phloem sap flows down a pressure gradient as hypothesised by Münch (1930). The amount of water that can flow through a unit area of phloem per unit time is proportional to permeability. The sap flow rate Q [m^3·s^{-1}] increases linearly with permeability k [m^2] and the area of phloem A_Φ [m^2]. It is predicted by Darcy's law:

$$Q = -\frac{k}{\mu} A_\Phi \frac{\Delta p}{\ell}. \quad (1)$$

The viscosity of phloem sap, μ [Pa·s], increases with sucrose concentration. The pressure gradient, $\frac{\Delta p}{\ell}$, corresponds to the pressure differential, Δp, between roots and leaves over the length of the stem ℓ, here taken as the measured tree height

We calculated phloem permeability by summing the hydraulic conductivities κ_i of all sieve cells (SCs) of each conducting phloem sample and dividing by the total sample's area of phloem (Equation 2). Conductivities are added because SCs are in parallel.

$$k = \frac{1}{A}\left(\sum_{i=1}^{n_S} \kappa_i\right), \tag{2}$$

where n_S is the number of SC present in a phloem sample of area A.

2.6.2 | Sieve Cell Conductivity

The hydraulic conductivity of an individual SC, κ, was calculated as the inverse of the sum of lumen's and cell wall's hydraulic resistances (Equation 3). The resistances are additive in series. SC conductivity can be written as a function of the lumen conductivity κ_L and the wall conductivity κ_W:

$$\kappa = \left(\frac{1}{\kappa_L} + \frac{1}{\kappa_W}\right)^{-1}. \tag{3}$$

We introduce the sieve-pore factor $S_p = 1 + \frac{\kappa_L}{\kappa_W}$ to reformulate SC conductivity as a function of lumen's conductivity only (Equation 4).

$$\kappa = \frac{\kappa_L}{S_p}. \tag{4}$$

The value of S_p represents the increase in hydraulic resistance associated to cell wall traversal (Jensen 2018). At $S_p = 1$, the conductivity would be equivalent to flow through an open-ended SC.

We assume that sap flow through a SC is a laminar viscous flow in a long channel and can be described by the Hagen-Poiseuille equation. The approach has been used to predict the hydraulic conductivity of sieve-tube elements and tracheids before (Thompson and Holbrook 2003; Pittermann et al. 2006) Unlike those studies, we use the Poiseuille's expression for channels with a rectangular cross-section, not circular, to match SC geometry(Mortensen et al. 2005):

$$\kappa_{\blacksquare} = \frac{\alpha d_T^4}{12}\left(1 - \frac{192}{\alpha \pi^5} \sum_{n=1,3,5,\ldots}^{\infty} \frac{1}{n^5} \tanh\left(\alpha n \frac{\pi}{2}\right)\right), \tag{5}$$

where d_T is the tangential diameter of the SC lumen, $\alpha = \frac{d_R}{d_T}$ is the rectangular aspect ratio, and ℓ is the channel's length. The SC cross-section is typically rectangular (Schulz 1992). Theoretical calculations assuming a circular section (Liesche et al. 2017; Jensen et al. 2012) overestimate lumen flow rates, that is, the flow rate in a circular channel is 13% higher than in a square one of equal cross-sectional area. In conifers, organelles remain present at lumen periphery after differentiation (Schulz 1992), potentially reducing the hydraulic diameter of the cell and increasing the resistance to flow. However, this effect was neglected in the model since the presence of organelles and their dimensions could not be determined reliably from the anatomical samples. The channel's length was taken as the SC's ℓ_S minus the overlapping length ℓ_O and the wall's ℓ_W, that is, $\ell_L = \ell_S - \ell_O - \ell_W$. The overlapping length was taken equal to half cell length (Pittermann et al. 2006): $\ell_O = \frac{\ell_S}{2}$. SC length was chosen equal to that of a 2-year-old *Pinus radiata* tracheid $\ell_S = 1500\ \mu$m (Burdon et al. 1992). SC length is assumed to match tracheid's length for a given age as both cell types divide from the same fusiform initials. The lumen conductivity is weighted by lumen's relative length as $\kappa_L = \frac{\ell_L + \ell_W}{\ell_L}\kappa_{\blacksquare}$.

Similarly, the wall conductivity in Equation 3 is weighted and is given by Equation 6.

$$\kappa_W = \frac{\ell_L + \ell_W}{\ell_W} n_p \kappa_{\therefore}, \tag{6}$$

where $\kappa_{\therefore}$ is the conductivity of a single pore, ℓ_W is the pore's length, and n_p is the total number of pores between two SCs. Pore's length was chosen to be one-third of the double cell wall thickness to represent the lack of secondary thickening at sieve-area sites in *Pinus radiata* (Barnett 1974b) and in *Pinaceae* (Evert 2006; Schulz 1992). The value of $\kappa_{\therefore}$ was calculated following Equation 7 which assumes a Poiseuille flow through the pore and introduces an additional term providing hydraulic resistance for thin pores (Thompson and Holbrook 2003).

$$\kappa_{\therefore} = \left(\frac{128}{\pi d_p^4} + \frac{24}{\ell_W d_p^3}\right)^{-1} \tag{7}$$

where d_p is the mean pore diameter. The number of pores was determined by Equation 8.

$$n_p = \frac{2\ell_O d_R \epsilon_A \epsilon_p}{\pi d_p^2}, \tag{8}$$

where ϵ_A is the fraction of radial wall area covered by sieve areas, ϵ_p is the fraction of a sieve area covered by pores, and d_R is the radial diameter of the SC. Most cell wall parameters could not be determined from the anatomical samples. We chose $\epsilon_A = 0.22$, approximately double the fraction of total wall area occupied by bordered pits in *Pinus* tracheids (Pittermann et al. 2006) as sieve areas are only present on radial walls in the genus. Sieve areas were assumed to have a low porosity ($\epsilon_p = 0.05$). For wall conductivity calculations we chose $d_p = 0.4\ \mu$m as an intermediate point in the 0.1-0.8 μm biological range (Schulz 1992). Because of natural variation, a sensitivity analysis was carried out for ℓ_S, d_T, $d_p$to measure the effect of parameter selection on SC hydraulic conductivity (Supporting material 1, Figure S1, Figure S2).

2.6.3 | Sap Flow Rate and Speed

The theoretical rate of phloem sap flow for all trees was calculated using Equation 1 after determining permeability from anatomical data. The pressure differential was chosen equal to 0.7 MPa (Jensen et al. 2012), the transport length was taken equal to individual plant height, and the viscosity was set equal to 0.005 Pa·s (Jensen et al. 2012). The mean phloem sap flow speed was derived from the volume flow rate using:

$$u = \frac{1}{\epsilon_\Phi A_\Phi} Q = -\frac{k}{\mu \epsilon_\Phi} \nabla p, \quad (9)$$

where ϵ_Φ is the fraction of the conducting phloem area occupied by SC.

3 | Results

3.1 | Main Effects of Shade and Pathogenic Infection

During the first sampling date, all shaded and infected (SI) plants showed the same percentage of brown needles as control plants (0%–25%), but at the second sampling date all SI plants presented a greater proportion of brown needles (25%–50%) than the control grafts (all presenting 0%–25%). We attributed the necrotic tissue to foliar pathogenic infection, as light-limited infected plants showed unequivocal lesions typical of *Dothistroma* needle blight and red needle cast (*Phytophthora pluvialis*) at both sampling dates. Light availability in the subcanopy of Kinleith forest was 7.8% of the light received by plants in the nursery, for the range 205–1408 $\mu mol \cdot m^{-2} \cdot s^{-1}$ (Figure S3). We used rapid light curves to translate the reduction in light availability into a reduction in *ETR*, by predicting *ETR* values using the fitted *gamm* model. Light reduction caused a loss in *ETR* of 89.7% with respect to nursery (control) values. Therefore, we could assume that at the shoot level, plants growing in subcanopy conditions were photosynthesising around 10% of the rate seen in control plants. Overall, photosynthate production was further reduced by an average crown loss of ca. 40% on average due to necrotic needles in stressed plants.

An Elastic Net analysis identified relative radial growth loss, NSC reserves in roots and stems and stomatal conductance as the key predictors of the growing conditions experienced by a given radiata pine plant in our experiment (Table 2). Diameter growth most effectively classified the plants by their growing condition. Secondary growth, estimated by the increase in diameter, classified growing conditions better than primary growth, estimated by the increase in height (Table 2). Lower NSC in roots appeared to be an indication of shaded growing conditions and pathogenic infection whereas greater soluble sugar pools in the stem were more tightly related to full sunlight growing conditions and healthy status. Understory-grown radiata pine plants showed higher stomatal conductance and transpiration than full sunlight grown plants (as shown by the positive parameter estimates, Table 2). Of all the phloem characteristics measured, phloem width responded most strongly to light and pathogen exposure. Another anatomical variable, the SC density, increased under light-limitation and pathogen exposure.

3.2 | Impact of Environmental Constraints on Phloem Anatomy of *Pinus radiata*

3.2.1 | Tissue Structure and Composition

Pinus radiata plants grown in full sunlight presented a larger phloem and higher total cell area in summer (December 19, 2017) than SI plants (Figures 2a and 3a), which were the main variables highlighted by the Elastic Net analysis regarding phloem changes. SC were the most abundant cell type in the inner phloem of *Pinus radiata*, irrespective of growing conditions (Figure S4). The total area of SC increased in sunlit plants from spring to summer whereas it remained constant in SI plants and equal to the spring value for sunlit plants (Figure 2b). Total cell density, and SC density in particular, were higher in SI than control plants, across samplings (1.7 and 1.3 higher, respectively, Figure 4a,b). However, a narrower phloem in SI plants resulted in a significantly lower area occupied by SC in early summer, when compared to control plants (Figure 2a).

The increase in SC density was related to the mean SC lumen area. There was a significant correlation between the log-transformed mean SC lumen area and the SC density in SI plants ($R^2 = 0.44$; $F_{1,\ 15} = 11.56$; $p = 0.004$; Figure S5). This correlation was weaker when including control plants ($R^2 = 0.26$; $F_{1,\ 29} = 10.39$; $p = 0.003$).

While the total area of AP cells did not change in response to growing conditions or sampling date, AP cell density decreased in summer across growing conditions (Figure 4c). TP cells showed significantly lower total area in understory-grown plants since spring (Figure 2c,d), even though their TP cell density was significantly higher compared to control plants in summer (Figure 4d). Some TP cells in phloem of SI plants appeared emptied from cellular contents in summer (7.6% of TP

TABLE 2 | Parameter estimates for the standardised variables that are selected by the elastic net analysis, explained deviance of the corresponding individual *glm* models, *p* values and corrected *p* values using the BH method.

Variable	Variable type	Parameter estimate	Explained deviance	*p* value	Corrected *p* value
Diameter growth	Growth	−0.320	0.666	0.014	0.016
NSC in roots	C reserves	−0.238	0.568	0.007	0.012
SS in stems	C reserves	0.193	0.393	0.005	0.012
g_s	Gas exchange	0.130	0.453	0.005	0.012
Phloem width	Phloem anatomy	−0.037	0.255	0.008	0.012
Height growth	Growth	−0.031	0.352	0.020	0.020
Transpiration	Gas exchange	0.023	0.326	0.009	0.012
SC density	Phloem anatomy	0.023	0.366	0.007	0.012

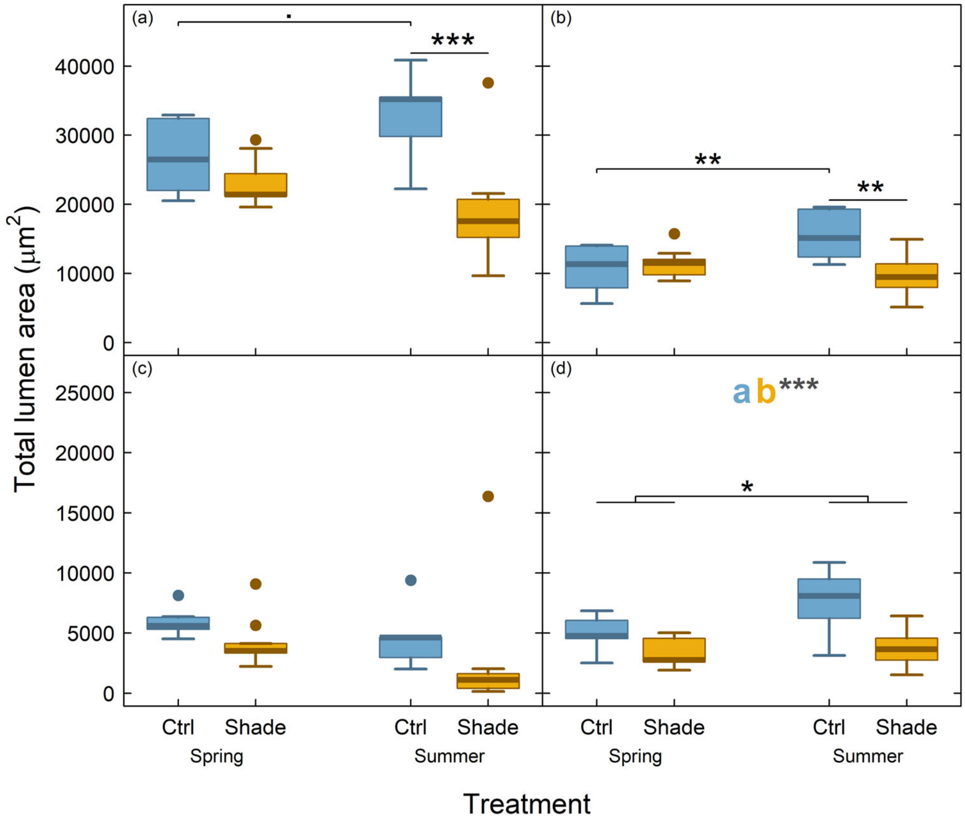

FIGURE 2 | Total lumen area of (a) all phloem cells, (b) sieve cells, (c) axial parenchyma cell, and (d) tannin-filled axial parenchyma cells for full sunlight-grown (blue) and shaded and pathogen-infected (orange) plants. Different blue and orange letters show significant differences between control (Ctrl) and shaded (Shade) plants regardless of the sampling date from the *glm* or *lm* models at: · $p < 0.1$; *$p < 0.05$; **$p < 0.001$; ***$p < 0.0001$. [Color figure can be viewed at wileyonlinelibrary.com]

presenting this condition in SI plants, vs. 0.9% in control plants; $z_{2,\ 31} = 7.97$; $p < 0.001$, *glm* model, family Poisson). An example of the studied phloem sections with identified cell types is shown in Figure 5.

3.2.2 | Individual SC Geometry

There was no difference in the mean aspect ratio and its distribution between control and SI plants. Individual SC displayed a rectangular cross-section with a mean aspect ratio of $\alpha = \frac{2}{3}$. The mean ratio corresponds to a tangential diameter 50% greater than the radial diameter on average (Figure S6). Most SC population showed that bias towards a larger tangential diameter as emphasised by the inter-quartile range $\mathrm{IQR}(\alpha) = \left[\frac{1}{2}, \frac{5}{6}\right]$. Despite that trend, 20% of SC displayed a greater diameter in the radial direction. Overall, the cross-sectional shape varied broadly ($\alpha = \frac{1}{5}$, first percentile to $\alpha = \frac{3}{2}$, last percentile).

For the most frequent aspect ratio, $\alpha = \frac{2}{3}$, the flow rate in a SC lumen is 7% lower than for a SC lumen with a square cross-section ($\alpha = 1$) and 21% lower than one with a circular cross-section. This implies that the typical SC cross-sectional geometry is suboptimal for phloem sap transport in the lumen but the loss in efficiency is small. When compounding end-wall hydraulic resistance (Figure S6), the mean aspect ratio of SC appears more detrimental to hydraulic efficiency. The maximum theoretical flow rate would instead be achieved when the radial diameter is approximately 50% greater than the tangential one, which is an extremely rare occurrence. This asymmetrical behaviour of SC flow rate with aspect ratio occurs because sieve areas are only present on the radial walls.

3.3 | Impact of Environmental Constraints on Phloem Hydraulic Properties

Phloem permeability was also impacted by growing conditions, being higher in SI plants regardless of sampling dates (Figure 3b). In part, this could be explained by a lower mean SC wall thickness in SI than control plants (Figure 3c). SC wall thickness remained consistent regardless of the distance from the cambium (see Supporting material 2 and Figure S7). Likewise, there were no observed differences in SC lumen area, and no distinct AP cells were found separating early and late phloem. As a result, we could not differentiate between the formation of early and late phloem cells.

Theoretical phloem sap velocity showed did not appear to be affected by growing conditions and sampling date (Figure 6a). Sap speed represents the intrinsic ability of the phloem to conduct sap, independent of the amount of conductive tissue and primarily depends on permeability and porosity for a given pressure gradient. It is a useful distinction from the sap flow rate, which incorporates phloem size and represents the

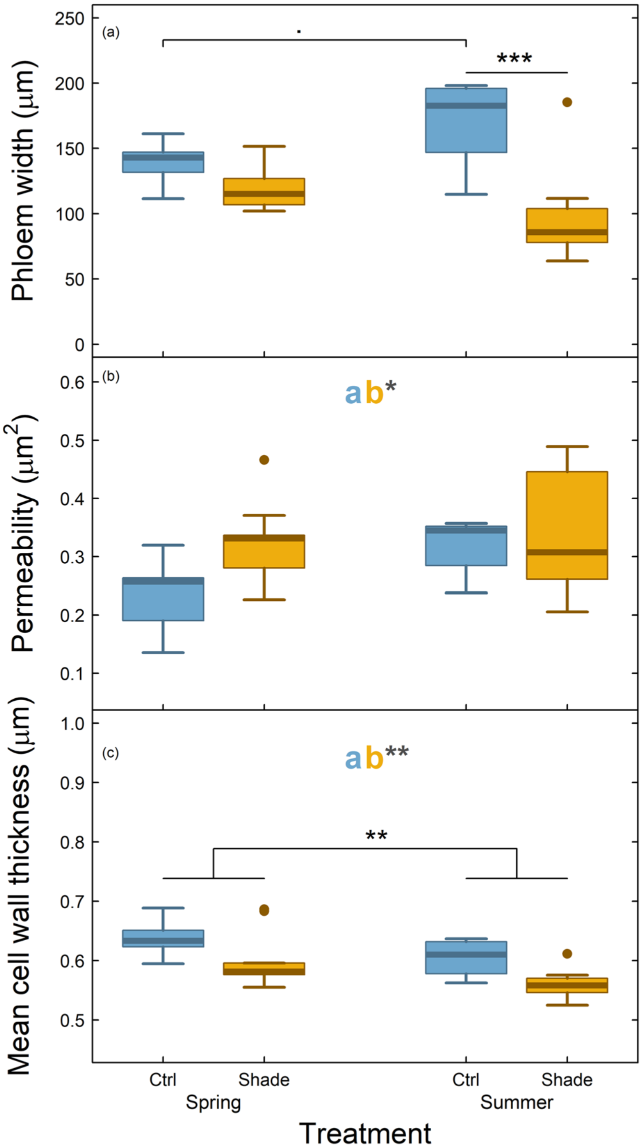

FIGURE 3 | Phloem anatomy features for full sunlight-grown (blue) and shaded and pathogen-infected (orange) plants: (a) phloem width, (b) permeability computed following Equation 2, and (c) sieve cell wall thickness. Different blue and orange letters show significant differences between control (Ctrl) and shaded (Shade) plants regardless of the sampling date from the *glm* or *lm* models at: · $p < 0.1$; *$p < 0.05$; **$p < 0.001$; ***$p < 0.0001$. [Color figure can be viewed at wileyonlinelibrary.com]

absolute transport efficiency. When considering the cross-sectional phloem area, SI plants presented a narrower phloem and consequently a lower mass flow rate than control plants (Figure 6b). Those differences became apparent in summer, similarly to differences in phloem width (Figure 3a).

3.4 | Impact of Environmental Constraints on Gas Exchange and Nonstructural Carbohydrates

According to the results of the Elastic Net model, stomatal conductance was the most important gas-exchange variable impacted by the growing conditions (Table 2) in the two sampling dates (Figure 7a). SI plants showed higher stomatal conductance, with average values of 194.7 versus 457.9 $\text{mmol·m}^{-2}\text{·s}$, in control and SI plants respectively. In contrast, net photosynthesis was similar across treatments (Figure 7b), with average values ranging from 9.8 $\mu\text{mol·m}^{-2}\text{·s}$ for control plants in spring to 13.8 $\mu\text{mol·m}^{-2}\text{·s}$ for SI plants in summer. The quantum yield of photosystem II and the *ETR* were significantly lower in plants grown under reduced light availability (Figure 7c).

Control plants showed higher starch content in needles than SI plants (22.1% decrease in SI individuals relative to control plants across dates; Figure 8d), which in turn presented higher soluble sugar content in needles in summer (20.8% increase in SI respect to control plants in summer; Figure 8a). Starch content in stem and soluble sugar content in stem and roots were higher in stressed plants only in spring (Figure 8b,c,e). In summer, starch and soluble sugars in stems and roots did not differ significantly among growing conditions (Figure 8b,c,e,f).

4 | Discussion

We studied the impact of reduced light availability and foliar pathogenic infection on phloem function, a combination of factors whose impact on phloem has not been studied before. With our monitoring of phloem twice in the same year (spring and summer), when radiata pine's cambial activity peaks in New Zealand (Nanayakkara et al. 2019), we showed that phloem development responds to environmental constraints within the same growing season comparing genets of the same clone. Although we could not distinguish between cells formed during the previous and current growing seasons, the genets experienced identical growing conditions until the onset of treatments. Therefore, the anatomical differences observed in this study must be mainly attributed to those treatments. In our study, we report phloem anatomy and hydraulic values for radiata pine, being consistent with previous reports, under no environmental stress (Barnett 1974a, 1974b; Cronshaw 1981). We observed changes in phloem anatomy (increased SC density and permeability, and reduced cell wall thickness) directed towards an improved phloem hydraulic function in the first sampling date in SI plants. While these changes were still present in the second sampling date, SI plants showed an eventual decrease in sap flow rate mediated by the reduction of phloem width. Stressed plants presented a remarkable impact in several physiological parameters, such as C assimilation, growth and phloem hydraulic function.

4.1 | Phloem Developmental Response to Stress

Environmental constraints associated with subcanopy growth conditions induced changes in phloem characteristics within a month. Those changes became significantly more pronounced over time and encompassed several anatomical features of the functioning tissue. Phloem width reduction was the most significant of those changes along with the decrease in total SC lumen area. Phloem width increased by 20% from spring to summer in sunlit plants, which translated to a theoretical sap

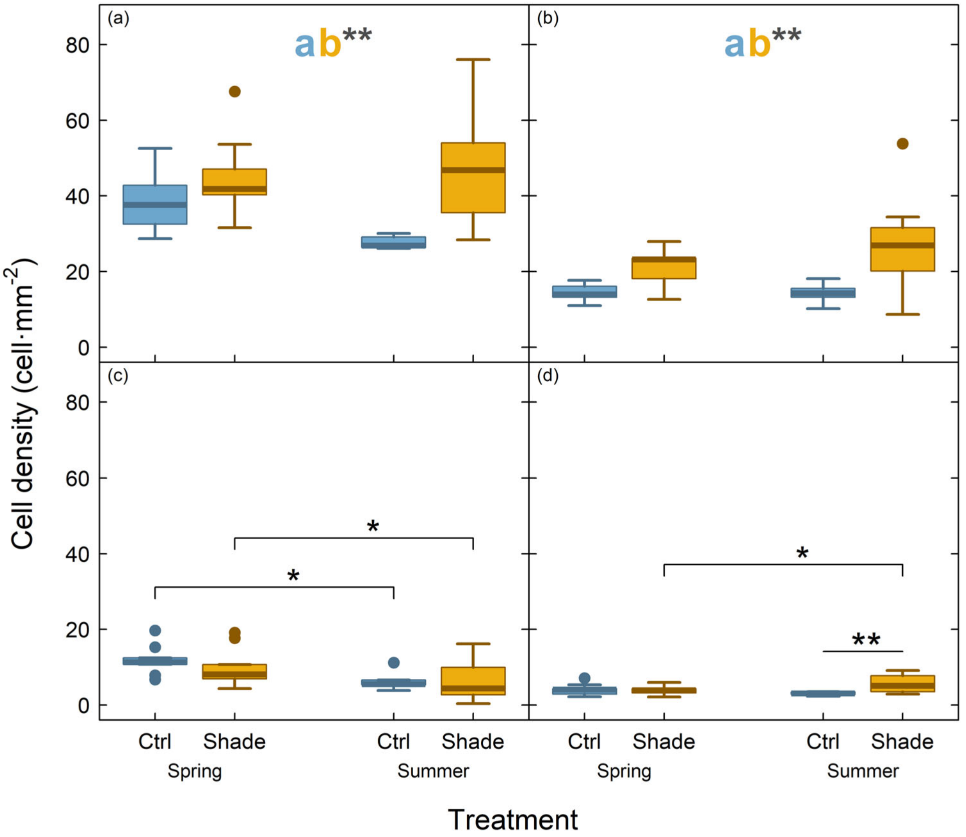

FIGURE 4 | Cell density (of a) all phloem cells, (b) sieve cells, (c) axial parenchyma cell, and (d) tannin-filled axial parenchyma cells for full sunlight-grown (blue) and shaded and pathogen-infected (orange) plants. Different blue and orange letters show significant differences between control (Ctrl) and shaded (Shade) plants regardless of the sampling date from the *glm* or *lm* models at: · $p < 0.1$; *$p < 0.05$; **$p < 0.001$; ***$p < 0.0001$. [Color figure can be viewed at wileyonlinelibrary.com]

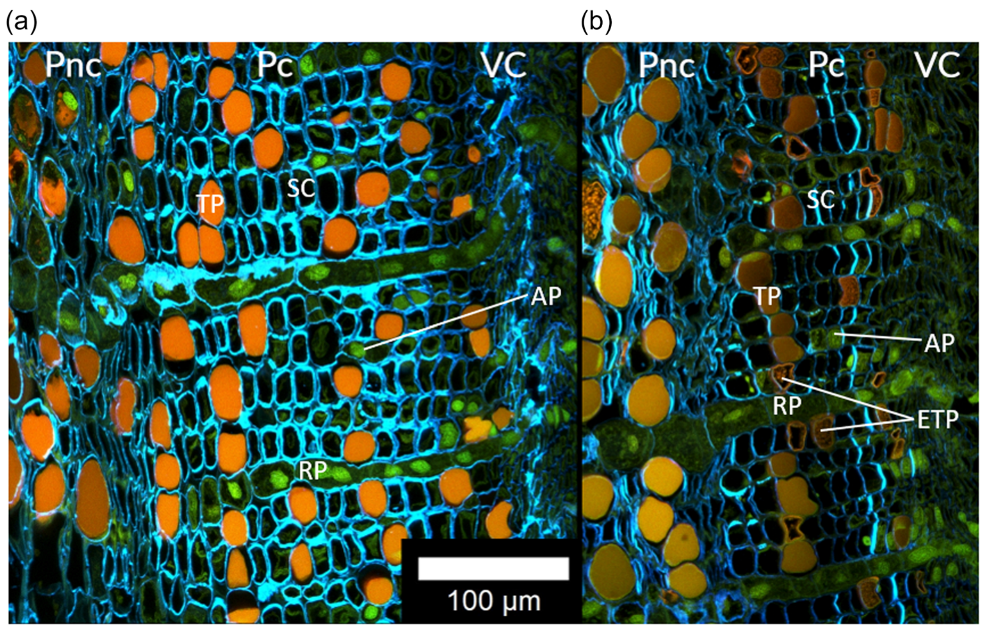

FIGURE 5 | Confocal laser scanning microscope images of phloem of (a) full sunlight-grown and (b) a shaded and pathogen-infected plant. Bar = 100 μm. AP, axial parenchyma cells; ETP, emptied tannin-filled parenchyma cells; Pc, conducting phloem; Pnc, nonconducting phloem; RP, ray parenchyma cells; SC, sieve cells; TP, tannin-filled parenchyma cells; VC, vascular cambium. [Color figure can be viewed at wileyonlinelibrary.com]

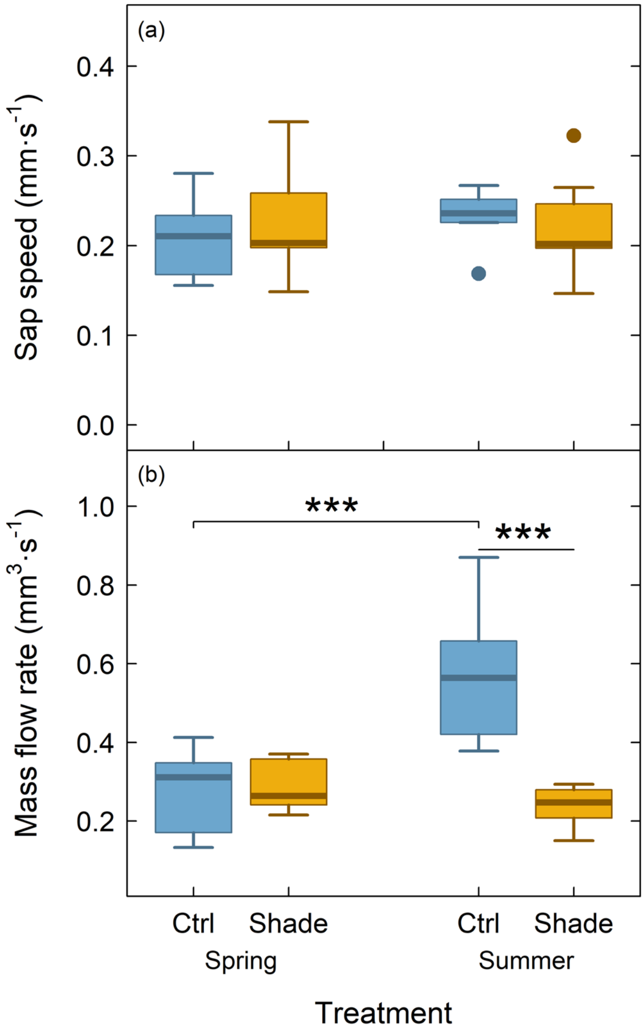

FIGURE 6 | Phloem hydraulic features for full sunlight-grown (blue) and shaded and pathogen-infected (orange) plants: (a) sap speed, and (b) sap mass flow rate. Significant differences from the *glm* or *lm* models only when specified: $^{***}p < 0.0001$. [Color figure can be viewed at wileyonlinelibrary.com]

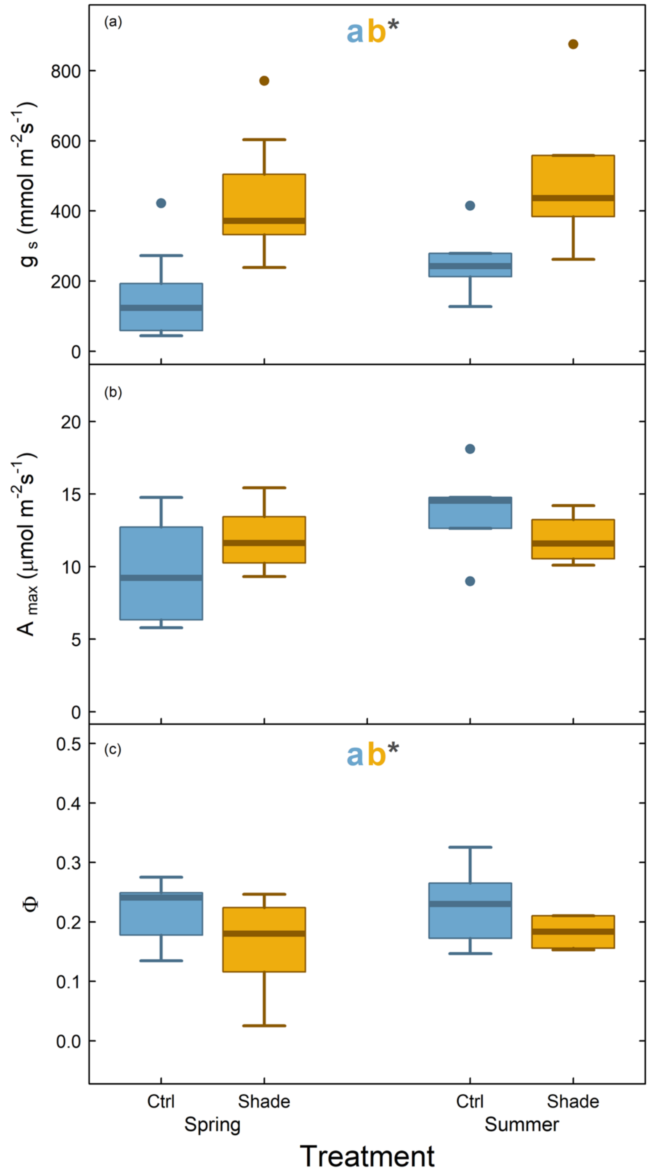

FIGURE 7 | Gas exchange parameters measured at saturating *PPFD* for full sunlight-grown (blue) and shaded and pathogen-infected (orange) plants: (a) stomatal conductance, (b) photosynthetic capacity, and (c) apparent quantum yield. Different blue and orange letters show significant differences between control (Ctrl) and shaded (Shade) plants regardless of the sampling date. [Color figure can be viewed at wileyonlinelibrary.com]

flow rate in summer that was twice the spring value. Phloem width of SI plants was only 58% of that in control plants in summer, implying a considerable reduction in transport efficiency due to growing conditions. Even though phloem cell formation has been shown to be mainly endogenously controlled (Prislan et al. 2013; Swidrak et al. 2014), some degree of plasticity in phloem formation and in anatomical features has been previously reported (Gričar et al. 2009; Yu et al. 2021; Gričar et al. 2014, 2015, 2022, 2024). Those studies have mainly established the impact of climate variables on phloem formation by comparing the same tree species across sites with differing weather conditions and varying elevations. An essential point in our study is that we controlled the genetic variability and local adaptation that might affect tree responses to environmental fluctuations, by using the same genotype grown under the same conditions until being subjected to contrasting light conditions and exposure to pathogenic infection. Hence, our study emphasises that variation in phloem composition and width in radiata pine is driven by environmental constraints within the same growing season, rather than differences in the genetic makeup. The reduced phloem width in SI plants might have been induced directly by either the impact of environmental constraints on phloem cell formation or by a premature SC collapse.

Shade and pathogenic infection impacted other anatomical parameters as well as cell composition. Even though the total lumen area occupied by TP and SC was significantly lower than in control plants, they were more densely packed in SI plants. SC density was linked to the mean individual SC lumen area under stress, as previously reported for *Picea abies* (Jyske and Hölttä 2015). The size of SC has been reported to vary with precipitation (Gričar et al. 2024), and to decrease under drought stress (Dannoura et al. 2019). In our experiment, SC size was

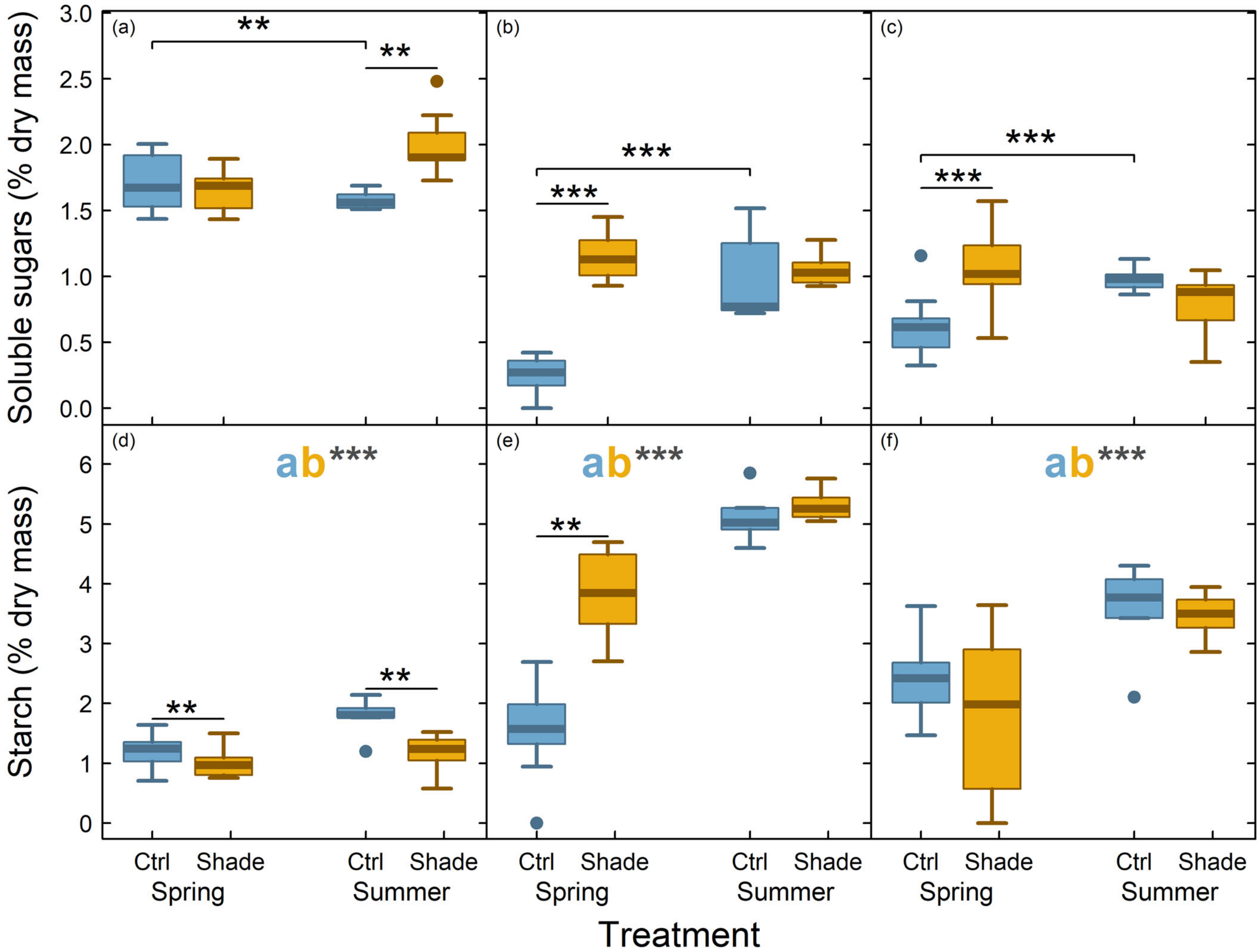

FIGURE 8 | Concentration of soluble sugars in (a) needles, (b) stem and (c) roots; and concentration of starch in (d) needles, (e) stem and (f) roots for full sunlight-grown (blue) and shaded and pathogen-infected (orange) plants. Different blue and orange letters show significant differences between control (Ctrl) and shaded (Shade) plants regardless of the sampling date from the *glm* or *lm* models at: $^{**}p < 0.001$; $^{***}p < 0.0001$. [Color figure can be viewed at wileyonlinelibrary.com]

not significantly different across treatments, but was reactive to SC density in SI *P. radiata*. In addition, SI plants displayed reduced cell wall thickness and increased permeability. The increase in permeability is particularly important as it corresponds to a relative increase in phloem transport efficiency per unit area of tissue. The higher SC density in SI plants failed to compensate for the drastic reduction in phloem width which resulted in a lower sap mass flow rate at the plant level. If we assume that no changes occurred on sieve pore areas, the reduced cell wall thickness seemingly increased the conductivity of individual cells. However, this increased permeability did not lead to an increase in whole-plant sap flow due to the reduced phloem size.

The impact of environmental constraints was more evident in summer than in spring. The variables that were impacted by the treatments since the earlier sampling date were the SC density, cell wall thickness and permeability. In the second sampling date, SC lumen area and phloem width became also different between SI and control plants (lower values of both variables in the latter). The actual negative impacts on phloem function were noticeable only late in the season (narrower phloem and lower SC lumen area), and the anatomical impacts in the first sampling date seemed to be directed to increase phloem hydraulic function. Thus, the increase in SC density and permeability and a decrease in cell wall thickness suggest an early response mechanism to stressful conditions aiming to maintain the overall performance of phloem transport under reduced C uptake in SI plants. However, these likely compensatory changes in phloem anatomy in SI plants did not appear sufficient to keep up with the plant-level flow rate of control plants. Early formation of phloem has been reported to be less affected by external meteorological conditions than late phloem, that reacts to environmental fluctuations (Gričar et al. 2009; Gričar and Čufar 2008). Here we show that shade and foliar pathogenic infection are important stressing factors in phloem formation and functioning that trigger, in the first place, changes to maintain hydraulic function as phloem formation is vital for tree survival (Gričar et al. 2009). As the combined stress continues, the impact observed later in the growing season is the opposite, and the response seems directed to adapt phloem cross-sectional area to a drastic reduction in C uptake.

TP cells were less abundant and tannins appeared less densely-stained in SI than control plants. The appearance of tannins has been suggested to vary as a function of the density of cell packing (Barnett 1974a), the molecular weight of polyphenolic compounds and also as a reaction to pathogen inoculation (Franceschi et al. 1998). Inoculation with *Ceratocystis polonica* induced a decrease in polyphenolic bodies in the polyphenolic parenchyma cells of *Picea abies* in a resistant clone, but less dramatically in a susceptible clone (Della Rocca et al. 2021; Franceschi et al. 1998). *C. polonica* colonises cambium and sapwood, but the pathogen infection reported in our plants was only by foliar pathogens, and no vascular pathogens were found. Therefore, in our experiment TP cells were not directly confronted to the presence of the pathogen in the stem, where phloem samples were taken from. We suggest that tannin compounds in our experiment could have presumably been mobilised away from TP to naturally-infected needles to face infection in our subcanopy-grown plants, as the phloem has been recognised as a highway for the transport of defensive metabolites (Heil and Ton 2008; Savage et al. 2016; Turgeon and Wolf 2009).

4.2 | Whole-Plant Response to Low Light Availability and Leaf Pathogenic Infection

Reduced light availability is a fairly common situation both for trees that have not reached a dominant position in the canopy, and for regenerating plants. A higher wetness in suppressed, as opposite to dominant, positions in a canopy creates better conditions for foliar pathogen infection, an additional stress for the plant to cope with. Reduced light and pathogen-induced lesions in needles led to reduced plant-level C uptake. Inversely, high light implies fast assimilation and accumulation of sugars in the needles. Shaded branches in broadleaf species have been reported to present reduced phloem area than sunlight branches on the same tree (Zhang et al. 2016). Theoretical modelling has also suggested that there is an optimal number of phloem sieve elements needed for phloem transport, which depends on the environmental conditions given a certain photosynthetic rate (Hölttä et al. 2009). This is consistent with our results in radiata pine, which shows that scaling of transport efficiency with photosynthesis can occur over a relatively short timeframe. Full sunlight-grown plants invested more in phloem area to maximise C fluxes at high light levels, while SI plants reduced phloem size as a potential adaptation to persistent low levels of C assimilation. SI plants were operating at light levels 92% lower than plants growing at full sunlight, which resulted in a decrease of 90% in the *ETR*. If we assume a similar reduction in C uptake, SI plants would have assimilated only one-tenth of the C assimilated by control plants, thus requiring much less phloem transport capacity. An additional decrease in C uptake occurred in summer because of pathogen-induced needle necrosis, affecting 25%–50% of the crown. As there is no evidence of compensatory upregulation of needle-level photosynthesis in response to severe defoliation in radiata pine (Gomez-Gallego et al. 2020), the crown loss observed in our study must have further reduced the amount of phloem tissue required to match the supply rates.

Subcanopy growth led to an increase in stomatal conductance in plants when measured under saturated light conditions, without concomitant increase in photosynthetic capacity (A_{max}), apparent quantum yield or *ETR*, which were similar across growing conditions. These results indicate that light-saturated stomatal conductance in shade-acclimated *P. radiata* plants is decoupled from photosynthesis. Two different mechanisms of stomatal opening have been previously reported (Matthews et al. 2020): a blue-light stomatal response that operates in guard cells and is thought to be independent of mesophyll photosynthesis; and a red-light response by which stomatal conductance links to photosynthetic rates (but controversy exists, Lawson et al. 2008; von Caemmerer et al. 2004; Wang and Song 2008). Since photosynthesis is sink-regulated (e.g., Körner 2015), the low growth-related C demand in our understory plants can readily explain the observed decoupling of photosynthetic C uptake from stomatal conductance (discussed in more detail below).

After 3 months of light deprivation and exposure to pathogens, SI plants unexpectedly showed NSC levels very similar to healthy plants grown in full light (Figure S8). The starch concentrations were comparable between treatments at the whole plant level (data not shown), suggesting that the drastic decrease in C uptake neither hindered the formation of C reserves for the late growing season, nor did it require their mobilisation to prevent carbon starvation. The concentration of soluble sugars in stem and roots were also very similar in both growing conditions, which indicates that C was locally available in those organs, probably as a consequence of reduced growth and (nearly zero) cambial sink activity. However, our findings may also indicate a systemic shift in C allocation driven by a declining C balance, as recently reported for Norway spruce, where C allocation to reserves took precedence over growth under photosynthesis-limiting conditions (Huang et al. 2021). The high levels of NSC observed in our experiment are an important finding that establishes that radial growth cessation and, by association, phloem formation impairment are not induced by the lack of carbohydrate supply to the meristem but precedes it. This is in general agreement with the sink-driven paradigm of plant growth (Fatichi et al. 2013; Körner 2003). The remarkable 25% increase in soluble sugars in the needles of understory-grown plants compared to the control, may indicate impaired phloem transport resulting from an accumulation of unexported C at the source. There are two likely explanations for this: on the one hand, reduced cambial activity could have caused reduced translocation through waning phloem unloading at sink sites. On the other hand, the build-up of soluble sugars in needles may reflect increased allocation to C-rich defensive compounds, linked to an upregulation of the tree defence system. Even in symptomless needles, we cannot rule out the pathogen's presence in the early stages of the infection. Further, the infection of neighbouring needles may have triggered an induced defence response and hence a growing defence sink. An increase in needle sugar concentrations is typically associated with an activation of inducible defences (Morkunas and Ratajczak 2014).

5 | Conclusion

Our findings highlight the impact of understudied environmental constraints, reduced light availability and foliar pathogenic infection, on radiata pine ecophysiology with a focus on phloem anatomy and function. Those environmental constraints are widespread in natural and planted forest ecosystems. In this study, we only examined phloem tissue of the stem of radiata pine grafts, but not from roots. We acknowledge the complexity of responses depending on the tissue and the age of the individual. The phloem response to the environmental challenges observed in this study reflects that of mature radiata pine branches, since we used the grafts derived from scions taken from mature radiata pine trees (Sweet 1972). Phloem formation in *P. radiata* was shown to respond strongly to those constraints in a severely modified environment emphasising a pronounced exogenous control. Phloem transport efficiency was primarily controlled by phloem size and the amount of conducting tissue. Phloem anatomy remained relatively unchanged but revealed minor changes in cell composition and characteristics that could have enhanced phloem function under stress. Those effects would be secondary and compensatory in nature compared to size effects. Phloem formation appeared to be dynamically adjusted to the reduction of C uptake as it varied with the amount of available light and necrotic foliage tissue. The mechanism by which phloem formation was controlled is unclear. It is possible that phloem formation control was intrinsically linked to cambial activity. Radial growth, unlike whole-plant functioning, was rapidly and severely impacted by the stressors. However, the reduced phloem size and growth inhibition were not triggered by a lack of available carbohydrates in the stem and root tissues. Locally available C was similar in stressed and unstressed plants and starch reserves did not seem to be mobilised.

SI plants seemed to have entered an impaired ecophysiological functioning with potential impacts on future survival, as shown by radial growth cessation, decelerated sap flow rate and sugar accumulation in needles. We suggest that, in the foliage of suppressed radiata pine trees or in the lower crown of dominant trees, both prone to foliar pathogen infection (Hood et al. 2022), physiological and structural alterations can occur on a regular basis. We speculate that the compounded impact of those alterations could lead to legacy effects on tree growth and vulnerability to additional stressors and, if frequent enough, jeopardise tree survival. In addition to understanding the compounding effects of abiotic and biotic stressors, the findings presented here have significant implications for the understanding of plant defence, breeding for resistance and epidemiological drivers of infection in the understorey. Our study demonstrates that studies of foliar pathogens in forest systems should consider the role of light limitation and plant physiological compensation as key components of plant-pathogen ecophysiology.

Acknowledgements

This study was supported by the MBIE research programme 'Healthy Trees Healthy Future' (C04X1305) and by the joint PHC/Dumont d'Urville (DDU-FRI1601) fund. The authors thank Donna Smith for embedding phloem samples in resin and Fiona Dean for imaging them.

Data Availability Statement

The data that support the findings of this study are available from the corresponding author upon reasonable request.

References

Abramoff, M. D., P. J. Magelhaes, and S. J. Ram. 2004. "Image Processing With ImageJ." *Biophotonics International* 11, no. 7: 36–42.

Angyalossy, V., R. Evert, C. Marcati, et al. 2016. "IAWA List of Microscopic Bark Features." *IAWA J. Int. Assoc. Wood Anat* 37: 517–615. https://doi.org/10.1163/22941932-20160151.

Barnett, J. R., 1971. Anatomical Studies and Evidende for Continuing Activity in *Pinus radiata* D. Don Cambium at Mid-Winter. For. Prod. Rep. No 354.

Barnett, J. R. 1974a. "Secondary Phloem in *Pinus radiata* D. Don. 2. Structure of Parenchyma Cells." *New Zealand Journal of Botany* 12: 261–274. https://doi.org/10.1080/0028825X.1974.10428870.

Barnett, J. R. 1974b. "Secondary Phloem in *Pinus radiata* D. Don: 1. Structure of Differentiating Sieve Cells." *New Zealand Journal of Botany* 12: 245–260. https://doi.org/10.1080/0028825X.1974.10428869.

Bassanezi, R. B., L. Amorim, A. B. Filho, and R. D. Berger. 2002. "Gas Exchange and Emission of Chlorophyll Fluorescence During the Monocycle of Rust, Angular Leaf Spot and Anthracnose on Bean Leaves as a Function of Their Trophic Characteristics." *Journal of Phytopathology* 150: 37–47. https://doi.org/10.1046/j.1439-0434.2002.00714.x.

Bauer, H., K. Plattner, and W. Volgger. 2000. "Photosynthesis in Norway Spruce Seedlings Infected by the Needle Rust *Chrysomyxa rhododendri*." *Tree Physiology* 20: 211–216. https://doi.org/10.1093/treephys/20.3.211.

Van Bel, A. J., Y. Helariutta, G. A. Thompson, et al. 2013. "Phloem: The Integrative Avenue For Resource Distribution, Signaling, and Defense." *Frontiers in Plant Science* 4: 471. https://doi.org/10.3389/fpls.2013.00471.

Bendix, C., and J. D. Lewis. 2018. "The Enemy Within: Phloem-Limited Pathogens." *Molecular Plant Pathology* 19: 238–254. https://doi.org/10.1111/mpp.12526.

Benjamini, Y., and Y. Hochberg. 1995. "Controlling the False Discovery Rate: A Practical and Powerful Approach to Multiple Testing." *Journal of the Royal Statistical Society Series B: Statistical Methodology* 57: 289–300. https://doi.org/10.1111/j.2517-6161.1995.tb02031.x.

Berger, S., A. K. Sinha, and T. Roitsch. 2007. "Plant Physiology Meets Phytopathology: Plant Primary Metabolism and Plant Pathogen Interactions." *Journal of Experimental Botany* 58: 4019–4026. https://doi.org/10.1093/jxb/erm298.

Bert, D., J. B. Lasnier, X. Capdevielle, A. Dugravot, and M. L. Desprez-Loustau. 2016. "Powdery Mildew Decreases the Radial Growth of Oak Trees With Cumulative and Delayed Effects Over Years." *PLoS One* 11: e0155344. https://doi.org/10.1371/journal.pone.0155344.

Bond, B. J., B. T. Farnsworth, R. A. Coulombe, and W. E. Winner. 1999. "Foliage Physiology and Biochemistry in Response to Light Gradients in Conifers With Varying Shade Tolerance." *Oecologia* 120: 183–192. https://doi.org/10.1007/s004420050847.

Brown, A., and R. W. Heckman. 2021. "Light Alters the Impacts of Nitrogen and Foliar Pathogens on the Performance of Early Successional Tree Seedlings." *PeerJ* 9: e11587. https://doi.org/10.7717/peerj.11587.

Bulman, L. S. 1993. "Cyclaneusma Needle Cast and Dothistroma Needle Blight in NZ Pine Plantations." *N. Z. For.* 38: 21–24.

Burdon, R. D., M. H. Bannister, and C. B. Low. 1992. "Genetic Survey of Pinus Radiata. 2: Population Comparisons for Growth Rate, Disease Resistance, and Morphology." *New Zealand Journal of Forestry Science* 22, no. 2/3: 138–159.

von Caemmerer, S., T. Lawson, K. Oxborough, N. R. Baker, T. J. Andrews, and C. A. Raines. 2004. "Stomatal Conductance Does Not Correlate With Photosynthetic Capacity in Transgenic Tobacco With

Reduced Amounts of Rubisco." *Journal of Experimental Botany* 55: 1157–1166. https://doi.org/10.1093/jxb/erh128.

Cronshaw, J. 1981. "Phloem Structure and Function." *Annual Review of Plant Physiology* 32: 465–484. https://doi.org/10.1146/annurev.pp.32.060181.002341.

Dannoura, M., D. Epron, D. Desalme, et al. 2019. "The Impact of Prolonged Drought on Phloem Anatomy and Phloem Transport in Young Beech Trees." *Tree Physiology* 39, no. 2: 201–210. https://doi.org/10.1093/treephys/tpy070.

Dickson, A., B. Nanayakkara, D. Sellier, D. Meason, L. Donaldson, and R. Brownlie. 2017. "Fluorescence Imaging of Cambial Zones to Study Wood Formation in *Pinus radiata* D. Don." *Trees* 31: 479–490.

Epron, D., M. Dannoura, and T. Hölttä. 2019a. "Introduction to the Invited Issue on Phloem Function and Dysfunction." *Tree Physiology* 39, no. 2: 167–172. https://doi.org/10.1093/treephys/tpz007.

Epron, D., M. Dannoura, A. Ishida, and Y. Kosugi. 2019b. "Estimation of Phloem Carbon Translocation Belowground at Stand Level in a Hinoki Cypress Stand." *Tree Physiology* 39: 320–331. https://doi.org/10.1093/treephys/tpy016.

Evert, R. F. 2006. *Esau's Plant Anatomy: Meristems, Cells, and Tissues of the Plant Body: Their Structure, Function, and Development*. John Wiley & Sons.

Fatichi, S., S. Leuzinger, and C. Körner. 2013. "Moving Beyond Photosynthesis: From Carbon Source to Sink-Driven Vegetation Modeling." *New Phytologist* 201: 1086–1095.

Franceschi, V. R., T. Krekling, A. A. Berryman, and E. Christiansen. 1998. "Specialized Phloem Parenchyma Cells in Norway Spruce (*Pinaceae*) Bark Are an Important Site of Defense Reactions." *American Journal of Botany* 85: 601–615. https://doi.org/10.2307/2446529.

Fraser, S., M. Gomez-Gallego, J. Gardner, L. S. Bulman, S. Denman, and N. M. Williams. 2020. "Impact of Weather Variables and Season on Sporulation of *Phytophthora pluvialis* and *Phytophthora kernoviae*." *For. Pathol.* 2005: 1–15. https://doi.org/10.1111/efp.12588.

Ganthaler, A., H. Bauer, A. Gruber, M. Mayr, W. Oberhuber, and S. Mayr. 2014. "Effects of the Needle Bladder Rust (*Chrysomyxa rhododendri*) on Norway Spruce: Implications for Subalpine Forests." *European Journal of Forest Research* 133: 201–211. https://doi.org/10.1007/s10342-013-0770-6.

Gibson, I. A. S. 1972. "Dothistroma Blight of *Pinus radiata*." *Annual Review of Phytopathology* 10: 51–72.

Gómez-Gallego, M., M. K.-F. Bader, P. M. Scott, S. Leuzinger, and N. M. Williams. 2017. "*Phytophthora pluvialis* Studies on Douglas-Fir Require Swiss Needle Cast suppression." *Plant Disease* 101: 1259–1262.

Gomez-Gallego, M., N. Williams, S. Leuzinger, P. M. Scott, and M. K.-F. Bader. 2020. "No Carbon Limitation After Lower Crown Loss in *Pinus radiata*." *Annali di Botanica* 125, no. 6: 955–967. https://doi.org/10.1093/aob/mcaa013.

Gričar, J., Š. Jagodic, B. Šefc, J. Trajković, and K. Eler. 2014. "Can the Structure of Dormant Cambium and the Widths of Phloem and Xylem Increments be Used as Indicators for Tree Vitality?" *European Journal of Forest Research* 133: 551–562. https://doi.org/10.1007/s10342-014-0784-8.

Gričar, J., J. Jevšenak, K. Giagli, et al. 2024. "Temporal and Spatial Variability of Phloem Structure in *Picea abies* and *Fagus sylvatica* and Its Link to Climate." *Plant, Cell & Environment* 47: 1285–1299. https://doi.org/10.1111/pce.14811.

Gričar, J., J. Jevšenak, P. Hafner, et al. 2022. "Climatic Regulation of Leaf and Cambial Phenology in *Quercus pubescens*: Their Interlinkage and Impact on Xylem and Phloem Conduits." *Science of the Total Environment* 802: 149968. https://doi.org/10.1016/j.scitotenv.2021.149968.

Gričar, J., L. Krže, and K. Čufar. 2009. "Number of Cells in Xylem, Phloem and Dormant Cambium in Silver Fir (*Abies alba*), in Trees of Different Vitality." *IAWA Journal* 30: 121–133. https://doi.org/10.1163/22941932-90000208.

Gričar, J., P. Prislan, M. De Luis, et al. 2015. "Plasticity in Variation of Xylem and Phloem Cell Characteristics of Norway Spruce Under Different Local Conditions." *Frontiers in Plant Science* 6: 730. https://doi.org/10.3389/fpls.2015.00730.

Gričar, J., and K. Čufar. 2008. "Seasonal Dynamics of Phloem and Xylem Formation in Silver Fir and Norway Spruce as Affected by Drought." *Russian Journal of Plant Physiology* 55: 538–543. https://doi.org/10.1134/S102144370804016X.

Gričar, J., K. Čufar, K. Eler, et al. 2021. "Transition Dates From Earlywood to Latewood and Early Phloem to Late Phloem in Norway Spruce." *Forests* 12: 331. https://doi.org/10.3390/f12030331.

Hajji, M., E. Dreyer, and B. Marçais. 2009. "Impact of *Erysiphe alphitoides* on Transpiration and Photosynthesis in *Quercus robur* Leaves." *European Journal of Plant Pathology* 125: 63–72. https://doi.org/10.1007/s10658-009-9458-7.

Heil, M., and J. Ton. 2008. "Long-Distance Signalling in Plant Defence." *Trends in Plant Science* 13: 264–272. https://doi.org/10.1016/j.tplants.2008.03.005.

Hölttä, T., M. Kurppa, and E. Nikinmaa. 2013. "Scaling of Xylem and Phloem Transport Capacity and Resource Usage With Tree Size." *Frontiers in Plant Science* 4: 496. https://doi.org/10.3389/fpls.2013.00496.

Hölttä, T., M. Mencuccini, and E. Nikinmaa. 2009. "Linking Phloem Function to Structure: Analysis With a Coupled Xylem-Phloem Transport Model." *Journal of Theoretical Biology* 259: 325–337. https://doi.org/10.1016/j.jtbi.2009.03.039.

Hood, I. A., S. Husheer, J. F. Gardner, et al. 2022. "Infection Periods of *Phytophthora pluvialis* and *Phytophthora kernoviae* in Relation to Weather Variables and Season in *Pinus radiata* Forests in New Zealand." *New Zealand Journal of Forestry Science* 52: 17. https://doi.org/10.33494/nzjfs522022x224x.

Huang, J., A. Hammerbacher, J. Gershenzon, et al. 2021. "Storage of Carbon Reserves in Spruce Trees Is Prioritized Over Growth in the Face of Carbon Limitation." *Proceedings of the National Academy of Sciences* 118: 1–7. https://doi.org/10.1073/pnas.2023297118.

Huang, J., A. Rücker, A. Schmidt, et al. 2020. "Production of Constitutive and Induced Secondary Metabolites Is Coordinated With Growth and Storage in Norway Spruce Saplings." *Tree Physiology* 40: 928–942. https://doi.org/10.1093/treephys/tpaa040.

Imaji, A., and K. Seiwa. 2010. "Carbon Allocation to Defense, Storage, and Growth in Seedlings of Two Temperate Broad-Leaved Tree Species." *Oecologia* 162: 273–281. https://doi.org/10.1007/s00442-009-1453-3.

Jensen, K. H. 2018. "Phloem Physics: Mechanisms, Constraints, and Perspectives." *Current Opinion in Plant Biology* 43: 96–100.

Jensen, K. H., J. Lee, T. Bohr, H. Bruus, N. M. Holbrook, and M. A. Zwieniecki. 2011. "Optimality of the Münch Mechanism for Translocation of Sugars in Plants." *Journal of the Royal Society Interface* 8: 1155–1165. https://doi.org/10.1098/rsif.2010.0578.

Jensen, K. H., J. Liesche, T. Bohr, and A. Schulz. 2012. "Universality of Phloem Transport in Seed Plants." *Plant, Cell & Environment* 35: 1065–1076. https://doi.org/10.1111/j.1365-3040.2011.02472.x.

Jyske, T., and T. Hölttä. 2015. "Comparison of Phloem and Xylem Hydraulic Architecture in *Picea abies* Stems." *New Phytologist* 205: 102–115. https://doi.org/10.1111/nph.12973.

Knoblauch, M., J. Knoblauch, D. L. Mullendore, et al. 2016. "Testing the Münch Hypothesis of Long Distance Phloem Transport in Plants." *eLife* 5: e15341. https://doi.org/10.7554/eLife.15341.

Köppen, W. 1936. "Das Geographische System der Klimate." In *Handbuch Der Klimatologie* (1, Part C). Borntraeger Science Publishers.

Körner, C. 2003. "Carbon Limitation in Trees." *Journal of Ecology* 91: 4–17.

Körner, C. 2015. "Paradigm Shift in Plant Growth Control." *Current Opinion in Plant Biology* 25: 107–114. https://doi.org/10.1016/j.pbi.2015.05.003.

Kurokawa, H., Y. Kitahashi, T. Koike, J. Lai, and T. Nakashizuka. 2004. "Allocation to Defense or Growth in Dipterocarp Forest Seedlings in Borneo." *Oecologia* 140: 261–270. https://doi.org/10.1007/s00442-004-1566-7.

Lawson, T., S. Lefebvre, N. R. Baker, J. I. L. Morison, and C. A. Raines. 2008. "Reductions in Mesophyll and Guard Cell Photosynthesis Impact on the Control of Stomatal Responses to Light and CO_2." *Journal of Experimental Botany* 59: 3609–3619. https://doi.org/10.1093/jxb/ern211.

Liesche, J., M. R. Pace, Q. Xu, Y. Li, and S. Chen. 2017. "Height-Related Scaling of Phloem Anatomy and the Evolution of Sieve Element end Wall Types in Woody Plants." *New Phytologist* 214, no. 1: 245–256.

Malinowski, R., D. Singh, A. Kasprzewska, S. Blicharz, and A. Basińska-Barczak. 2024. "Vascular Tissue – Boon or Bane? How Pathogens Usurp Long-Distance Transport in Plants and the Defence Mechanisms Deployed to Counteract Them." *New Phytologist* 243: 2075–2092. https://doi.org/10.1111/nph.20030.

Manter, D. K., B. J. Bond, K. L. Kavanagh, P. H. Rosso, and G. M. Filip. 2000. "Pseudothecia of Swiss Needle Cast Fungus, *Phaeocryptopus gaeumannii*, Physically Block Stomata of Douglas fir, Reducing CO_2 Assimilation." *New Phytologist* 148: 481–491. https://doi.org/10.1046/j.1469-8137.2000.00779.x.

Manter, D. K., B. J. Bond, K. L. Kavanagh, J. K. Stone, and G. M. Filip. 2003. "Modelling the Impacts of the Foliar Pathogen, *Phaeocryptopus gaeumannii*, on Douglas-fir Physiology: Net Canopy Carbon Assimilation, Needle Abscission and Growth." *Ecological Modelling* 164: 211–226. https://doi.org/10.1016/S0304-3800(03)00026-7.

Martínez-Vilalta, J. 2014. "Carbon Storage in Trees: Pathogens Have Their Say." *Tree Physiology* 218: 228. https://doi.org/10.1093/treephys/tpu010.

Matthews, J. S. A., S. Vialet-Chabrand, and T. Lawson. 2020. "Role of Blue and Red Light in Stomatal Dynamic Behaviour." *Journal of Experimental Botany* 71: 2253–2269. https://doi.org/10.1093/jxb/erz563.

Minchin, P. E. H., M. R. Thorpe, and J. F. Farrar. 1993. "A Simple Mechanistic Model of Phloem Transport Which Explains Sink Priority." *Journal of Experimental Botany* 44: 947–955. https://doi.org/10.1093/jxb/44.5.947.

Morkunas, I., and L. Ratajczak. 2014. "The Role of Sugar Signaling in Plant Defense Responses Against Fungal Pathogens." *Acta Physiologiae Plantarum* 36: 1607–1619. https://doi.org/10.1007/s11738-014-1559-z.

Mullendore, D. L., C. W. Windt, H. Van As, and M. Knoblauch. 2010. "Sieve Tube Geometry in Relation to Phloem Flow." *Plant Cell* 22: 579–593. https://doi.org/10.1105/tpc.109.070094.

Münch, E., 1930. Die Stoffbewegungen in der Pflanze, Fischer Gustav.

Nanayakkara, B., A. R. Dickson, and D. F. Meason. 2019. "Xylogenesis of *Pinus radiata* D. Don growing in New Zealand." *Annals of Forest Science* 76: 74. https://doi.org/10.1007/s13595-019-0859-2.

Niinemets, Ü. 2007. "Photosynthesis and Resource Distribution Through Plant Canopies." *Plant, Cell & Environment* 30: 1052–1071. https://doi.org/10.1111/j.1365-3040.2007.01683.x.

Pinkard, E. A., and C. L. Mohammed. 2006. "Photosynthesis of *Eucalyptus globulus* With *Mycosphaerella* Leaf Disease." *New Phytologist* 170: 119–127. https://doi.org/10.1111/j.1469-8137.2006.01645.x.

Pinon, J., P. Frey, and C. Husson. 2006. "Wettability of Poplar Leaves Influences Dew Formation and Infection by *Melampsora larici-populina*." *Plant Disease* 90: 177–184. https://doi.org/10.1094/PD-90-0177.

Pittermann, J., J. S. Sperry, J. K. Wheeler, U. G. Hacke, and E. H. Sikkema. 2006. "Mechanical Reinforcement of Tracheids Compromises the Hydraulic Efficiency of Conifer Xylem." *Plant, Cell & Environment* 29, no. 8: 1618–1628.

Poorter, H., Ü. Niinemets, L. Poorter, I. J. Wright, and R. Villar. 2009. "Causes and Consequences of Variation in Leaf Mass Per Area (LMA): A Meta-Analysis." *New Phytologist* 182: 565–588. https://doi.org/10.1111/j.1469-8137.2009.02830.x.

Prislan, P., J. Gričar, M. De Luis, K. T. Smith, and K. Čufar. 2013. "Phenological Variation in Xylem and Phloem Formation in *Fagus sylvatica* From Two Contrasting Sites." *Agricultural and Forest Meteorology* 180: 142–151. https://doi.org/10.1016/j.agrformet.2013.06.001.

Ramirez, J. A., J. M. Posada, I. T. Handa, et al. 2015. "Near-Infrared Spectroscopy (NIRS) Predicts Non-Structural Carbohydrate Concentrations in Different Tissue Types of a Broad Range of Tree Species." *Methods in Ecology and Evolution* 6: 1018–1025. https://doi.org/10.1111/2041-210X.12391.

Rascher, U., M. Liebig, and U. Lüttge. 2000. "Evaluation of Instant Light-Response Curves of Chlorophyll Fluorescence Parameters Obtained With a Portable Chlorophyll Fluorometer on Site in the Field." *Plant, Cell & Environment* 23: 1397–1405. https://doi.org/10.1046/j.1365-3040.2000.00650.x.

R Core Team. 2023. "R: A Language and Environment for Statistical Computing." R Foundation for Statistical Computing. https://www.R-project.org/.

Della Rocca, G., I. Posarelli, F. Morandi, et al. 2021. "Different Polyphenolic Parenchyma Cell and Phloem Axial Resin Duct-Like Structure Formation Rates in *Cupressus sempervirens* Clones Infected With *Seiridium cardinale*." *Plant Disease* 105: 2801–2808. https://doi.org/10.1094/PDIS-01-21-0098-RE.

Saffell, B. J., F. C. Meinzer, D. R. Woodruff, et al. 2014. "Seasonal Carbohydrate Dynamics and Growth in Douglas-Fir Trees Experiencing Chronic, Fungal-Mediated Reduction in Functional Leaf Area." *Tree Physiology* 34: 218–228.

Salmon, Y., L. Dietrich, S. Sevanto, T. Hölttä, M. Dannoura, and D. Epron. 2019. "Drought Impacts on Tree Phloem: From Cell-Level Responses to Ecological Significance." *Tree Physiology* 39: 173–191. https://doi.org/10.1093/treephys/tpy153.

Savage, J. A., M. J. Clearwater, D. F. Haines, et al. 2016. "Allocation, Stress Tolerance and Carbon Transport in Plants: How Does Phloem Physiology Affect Plant Ecology?" *Plant, Cell & Environment* 39: 709–725. https://doi.org/10.1111/pce.12602.

Schulz, A. 1992. "Living Sieve Cells of Conifers as Visualized by Confocal, Laser-Scanning Fluorescence Microscopy." *Protoplasma* 166, no. 1992: 153–164.

Sevanto, S., ed. 2019. "Methods for Assessing the Role of Phloem Transport in Plant Stress Responses." In *Phloem: Methods and Protocols, Methods in Molecular Biology*. Springer New York. https://doi.org/10.1007/978-1-4939-9562-2.

Sweet, G. B. 1972. "The Effect of Maturation on the Growth and Form of Vegetative Propagules of Radiata Pine." *New Zealand Journal of Forestry Science* 3: 191–210.

Swidrak, I., A. Gruber, and W. Oberhuber. 2014. "Xylem and Phloem Phenology in Co-Occurring Conifers Exposed to Drought." *Trees* 28: 1161–1171. https://doi.org/10.1007/s00468-014-1026-x.

Tennent, R. B. 1986. "Intra-Annual Growth of Young *Pinus radiata* in New Zealand." *New Zealand Journal of Forestry Science* 16: 166–175.

Thompson, M. V., and N. M. Holbrook. 2003. "Scaling Phloem Transport: Water Potential Equilibrium and Osmoregulatory Flow." *Plant,* *Cell & Environment* 26: 1561–1577. https://doi.org/10.1046/j.1365-3040.2003.01080.x.

Toome, M., K. Heinsoo, and A. Luik. 2010. "Relation Between Leaf Rust (*Melampsora epitea*) Severity and the Specific Leaf Area in Short Rotation Coppice Willows." *European Journal of Plant Pathology* 126: 583–588. https://doi.org/10.1007/s10658-009-9566-4.

Turgeon, R., and S. Wolf. 2009. "Phloem Transport: Cellular Pathways and Molecular Trafficking." *Annual Review of Plant Biology* 60: 207–221. https://doi.org/10.1146/annurev.arplant.043008.092045.

Wang, P., and C.-P. Song. 2008. "Guard-Cell Signalling for Hydrogen Peroxide and Abscisic Acid." *New Phytologist* 178: 703–718. https://doi.org/10.1111/j.1469-8137.2008.02431.x.

Warrington, I. J., D. A. Rook, D. C. Morgan, and H. L. Turnbull. 1989. "The Influence of Simulated Shadelight and Daylight on Growth, Development and Photosynthesis of *Pinus radiata*, *Agathis australis* and *Dacrydium cupressinum*." *Plant, Cell & Environment* 12: 343–356. https://doi.org/10.1111/j.1365-3040.1989.tb01951.x.

Yasuda, Y., Y. Utsumi, X. Tan, N. Tashiro, K. Fukuda, and S. Koga. 2018. "Suppression of Growth and Death of Meristematic Tissues in *Abies sachalinensis* Under Strong Shading: Comparisons Between the Terminal Bud, the Terminally Lateral Bud and the Stem Cambium." *Journal of Plant Research* 131: 817–825. https://doi.org/10.1007/s10265-018-1051-8.

Yu, B., X. Li, P. Zhao, and J. Huang. 2021. "Comparison of Intra-Annual Xylem and Phloem Formation of *Picea crassifolia* Stands at Two Latitudes in Northwest China." *Forests* 12: 1445. https://doi.org/10.3390/f12111445.

Zhang, L., P. Copini, M. Weemstra, and F. Sterck. 2016. "Functional Ratios Among Leaf, Xylem and Phloem Areas in Branches Change With Shade Tolerance, but Not With Local Light Conditions, Across Temperate Tree Species." *New Phytologist* 209: 1566–1575. https://doi.org/10.1111/nph.13731.

Ziegler, H. 1975. "Nature of transported substances." In *Transport in Plants I. Phloem Transport., Encyclopedia of Plant Physiology*, 59–100. Springer.

Supporting Information

Additional supporting information can be found online in the Supporting Information section.